

Long-range exchange coupling in a magnetic multilayer system

L. O. Souza,* R. A. Dumer,† and M. Godoy‡

Instituto de Física - Universidade Federal de Mato Grosso, 78060-900, Cuiabá, Mato Grosso, Brazil.

In this study, we explored the magnetic coupling in a multilayer system consisting of thin layers separated by a distance d . We have employed Monte Carlo (MC) simulations to calculate the thermodynamic quantities such as the magnetization per spin m_L^μ , magnetic susceptibility χ_L^μ , and the reduced fourth-order Binder cumulant U_L^μ as a function of temperature T and for several values of lattice size L . These quantities were obtained for each layer ($\mu = l$), for the bulk system ($\mu = b$), as a function of interlayer distance d and the parameter α that defines the scale length of the exponential decay of the interaction. Furthermore, we applied the finite-size scaling theory to calculate the critical exponents. Our results reveal that the system exhibits 2D Ising exponents when the layers are sufficiently separated. On the other hand, in the compact limit, where d equals the distance between two adjacent sites within the same layer, our bulk results show that the system exhibits 3D Ising critical exponents, provided that the number of layers L_z increases proportionally to the layer sizes. Even with the separation increasing up to $d = 2.0$, the layers are so correlated that the set of critical exponents retains the values of 3D critical exponents. However, when the number of layers L_z remains fixed, even in the compact limit with periodic boundary conditions, only the exponent β aligns closely with the predicted literature values, on the other hand, the other exponents show significant deviations.

I. INTRODUCTION

Over the past thirty years, metallic spintronics has established itself as a significant field, with one of the most notable applications being the use of the Giant Magnetoresistance (GMR) effect in magnetic metallic multilayers for data storage [1, 2]. These materials feature ferromagnetic layers whose exchange coupling between adjacent layers oscillates in sign as the thickness of the non-magnetic spacer increases [3]. The next generation of spintronic materials aims to manipulate spin degrees of freedom at lower carrier densities and achieve control through applied electric voltages, with semiconductor-based materials expected to play a pivotal role, see, e.g., Refs. [4] and [5].

In this context, diluted magnetic semiconductors (DMS) have emerged as promising materials for generating spin-polarized carriers that can be manipulated for injection [6]. Among these, (Ga, Mn)As stands out as one of the most well-studied DMS. When a Mn atom substitutes a Ga atom, it introduces a localized magnetic moment along with one hole [6, 7]. However, many of these holes are compensated by defects. The remaining uncompensated holes interact antiferromagnetically with each Mn local moment, leading to ferromagnetic order below a critical temperature, $T_c(x)$, which varies non-monotonically with the concentration x of Mn [8].

Advances in experimental techniques have significantly increased the observed maximum critical temperature, from 60K [9] to 110K [8], and further improvements in post-growth annealing processes have pushed T_c to 184K [10]. Additionally, developments in deposition techniques

have enabled the growth of digital ferromagnetic heterostructures (DFH's), where submonolayer planes of MnAs are inserted into GaAs layers using molecular beam epitaxy [11]. Since holes can potentially correlate the magnetization in adjacent MnAs layers, a systematic study of interlayer coupling is essential.

With this in mind, we intend to investigate the interplay between the layering and ordering of localized magnetic moments placed regularly on equally spaced layers, coupled through hole-mediated exchange coupling. The broad features of this exchange coupling can be determined by following Refs. [12–14]. The long-range coupling constant of the form $J_{ij} = J_0 \exp(-2r_{ij}/a_B)$ [12], i.e., decaying algebraically with the interspin distance, that favors ferromagnetic ordering at low temperature. Here, J_0 defines the exchange energy scale, and a_B is the effective Bohr radius, for instance, with typical values for Mn in bulk GaAs being $J_0 = 15\text{meV}$ and $a_B = 7.8\text{\AA}$ [12]. Although this impurity band perspective may not be entirely suitable for low carrier densities, it nonetheless reflects the localized character of holes in (Ga,Mn)As [15]. Thus, when holes are integrated out, the interaction between pairs of localized spins primarily exhibits an exponential decay relative to their separation distance.

For magnetic models involving Heisenberg spins with significant quantum numbers (such as $S = 5/2$ for Mn spins, which considerably affect the magnetic response), the quantum corrections are typically minor. Therefore, we can use a classical vector spin model. In this context, considering the Ising spins and utilizing MC simulations is a reasonable approach [16, 17].

This paper is structured as follows. Section II, we detail the model used and outlines the MC simulation methods. Section III, we present and discuss the results. Finally, in Section IV, we display our conclusion with a summary of our findings.

* leandro.souza@fisica.ufmt.br

† rafaeldumer@fisica.ufmt.br

‡ mgodoy@fisica.ufmt.br

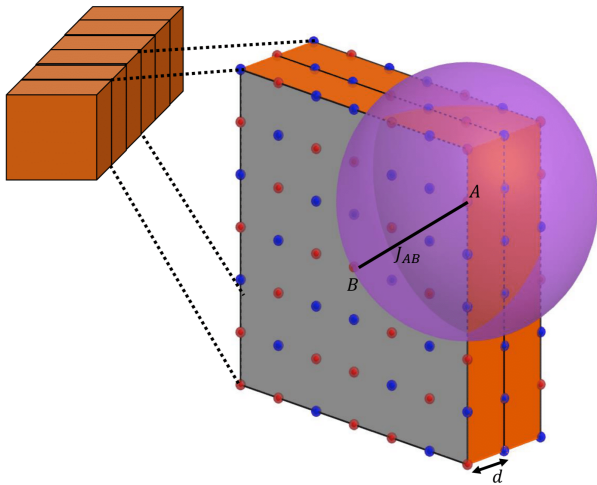


Figure 1. Schematic representation of a two-dimensional multilayers system with thickness d . J_{AB} is the long-range magnetic coupling $J(r_{ij})$ defined in Eq. 2.

II. MODEL AND METHODOLOGY

In line with our previous discussion, the classical spin Hamiltonian that we have studied is written by the following form:

$$\mathcal{H} = - \sum_{i,j} J(r_{ij}) S_i S_j, \quad (1)$$

where $S_i = \pm 1$ is the Ising spin variable at the position R_i of the lattice. While an oscillatory (i.e. alternating in sign) behavior of $J(r_{ij})$ has been ruled out by first-principles calculations [18, 19]. Therefore, it is instructive to investigate the effects of an additional power-law decay, which is reminiscent of the RKKY interaction [20–22]. That is, we propose a plausible configuration for the magnetic coupling $J(r_{ij})$:

$$J(r_{ij}) = \frac{J_0}{r_{ij}^3} \exp\left(-\frac{r_{ij}}{\alpha}\right), \quad (2)$$

where r_{ij} is the distance between the spins at site i and j , and $J(r_{ij})$ is the interaction strength. Here, the distance r_{ij} and the parameter α are expressed in units of the underlying lattice spacing, which, for our purposes here, it suffices to consider as being of the order of the effective Bohr radius a_B mentioned above. The sum in Eq. (1) is performed over all pairs spins. These atoms reside on L_z square lattice layers, each of which with $N = L \times L$ sites, and which are separated from each other by non-magnetic spacers of thickness d , as illustrated in Fig. 1.

The simulations, especially for large lattices, are extremely computationally costly, given that the interaction $J(r_{ij})$, as defined by Eq.(2), occurs among all sites

of the lattice. To overcome this limitation, we have set a cutoff in $J(r_{ij}^{\text{cutoff}})$ when the exponential decay has rendered the interactions sufficiently tenuous to be disregarded. Therefore, the interaction occurs within a cluster of spins smaller than the entire lattice. Let $N_{is}(R)$ be the number of new interactions that can be added at a site within an interaction radius R . Despite N_{is} increasing with the interaction radius R , as shown in Fig. 2(a), the value of $J(R)$ decays exponentially. For $R > 2.5$, the value of $J(R)$ falls below 3%, as demonstrated in Fig. 2(b). When considering the contribution of all interacting sites, as illustrated in Fig. 2(c), we can observe that setting a maximum radius as $R = 2.5$ is reasonable, since the most relevant interactions are among 94% of the entire lattice interaction. Thus, we set a cutoff in $J(r_{ij})$ for $r_{ij}^{\text{cutoff}} = 2.5$, i. e., in other words we have used $J(r_{ij} \geq 2.5) = 0$.

Since in the limit $d \rightarrow \infty$, the system presents a collection of independent planes. Therefore, in our MC simulations, we have calculated the thermodynamic quantities for each layer and the bulk system. Consequently, we can define the following parameter:

$$M_\mu = \sum_{i=1}^{N_\mu} S_i, \quad (3)$$

such that when the subscript $\mu = l$ and $\mu = b$ represent the layer and the bulk, respectively. For $\mu = l$, the sum runs over the $N_l = L^2$ sites within the layer and for $\mu = b$, the sum runs over the $N_b = N_l L_z = L^2 L_z$ sites within the bulk. We also have considered the k th-moment of the magnetization as

$$(m_L^\mu)^k \equiv \frac{1}{N_\mu^k} M_\mu^k. \quad (4)$$

The first-moment yields the magnetization per site,

$$m_L^\mu = \frac{1}{N_\mu} \left\langle \sum_{i=1}^{N_\mu} S_i \right\rangle, \quad (5)$$

magnetic susceptibility is given by

$$\chi_L^\mu = \frac{N_\mu}{k_B T} \left[\langle (m_L^\mu)^2 \rangle - (m_L^\mu)^2 \right], \quad (6)$$

In order to obtain the critical temperatures we can also use the fourth-order Binder cumulant [17]:

$$U_L^\mu = 1 - \frac{\langle m_\mu^4 \rangle}{3 \langle m_\mu^2 \rangle^2} \quad (7)$$

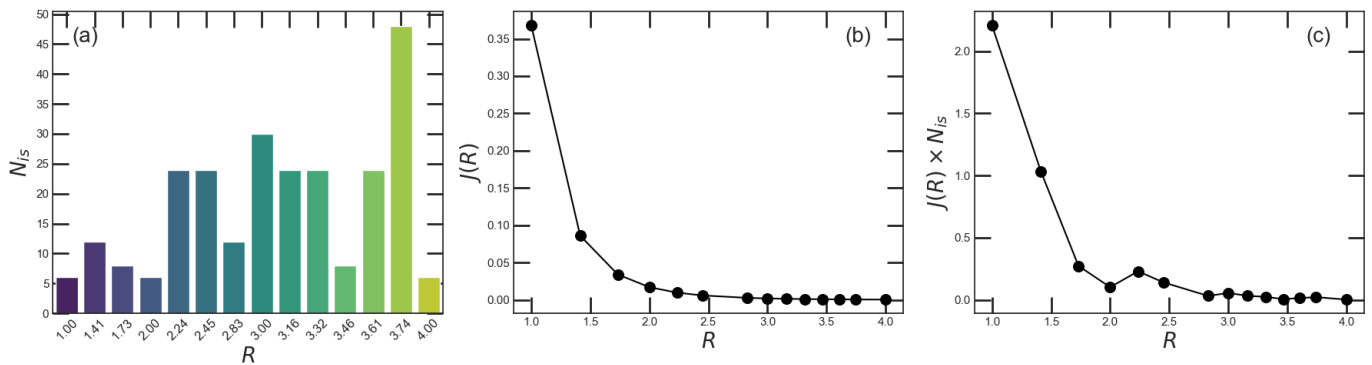


Figure 2. (a) Number of new interactions N_{is} as a function of radius R . (b) Magnetic couplings $J(R)$ as a function of the radius R . (c) Total contribution of the magnetic coupling $J(R) \times N_{is}$ for spins at a distance R . The plots (a), (b), and (c) were obtained for $\alpha = 1.0$ and $d = 1.0$.

where $\langle \dots \rangle$ denotes the thermal average over the MC simulation.

The magnetic layers are separated by non-magnetic spacers of thickness d , as illustrated in Fig. 1. We vary d and perform systematic MC simulations to calculate the thermodynamic quantities of interest (Fig. 3), and the critical exponents for the layers and the bulk.

Near the critical temperature T_c , the previously defined quantities conform to the finite-size scaling relations as follows:

$$m_L^\mu = L^{-\beta/\nu} m_0(L^{1/\nu} \epsilon), \quad (8)$$

$$\chi_L^\mu = L^{\gamma/\nu} \chi_0(L^{1/\nu} \epsilon), \quad (9)$$

$$U_L^{\mu'} = L^{1/\nu} U_0(L^{1/\nu} \epsilon) / T_c, \quad (10)$$

where $\epsilon = (T - T_c) / T_c$. In the equations above $m_0(L^{1/\nu} \epsilon)$, $\chi_0(L^{1/\nu} \epsilon)$, and $U_0(L^{1/\nu} \epsilon)$ are the scaling functions, and β , γ , and ν are the critical exponents for magnetization, magnetic susceptibility, and length correlation, respectively, and $U_L^{\mu'}$ is the derivative of U_L^μ with relation to T .

III. RESULTS AND DISCUSSION

In the following, we have considered layers with linear sizes ranging from $10 \leq L \leq 20$, while the stack size is fixed at $L_z = 10$. Additionally, we examined the cases where $10 \leq L_z \leq 20$ with $L_z = L$, $N_l = L^2$, and $N_b = L_z N_l = LL^2 = L^3$. We have allowed from 10^5 to 10^6 MC steps/spin to reach equilibrium, and averages have been obtained over 10^6 to 10^7 steps/spin. Fig. 3 illustrates the temperature dependence of some bulk thermodynamic quantities, with the parameter $\alpha = 1.0$ and

the interlayer distance $d = 1.0$, for several lateral sizes L and $L_z = 10$. In Fig. 3(a), we display the Binder cumulant, where we can observe that this quantity tends to $2/3$ deep in the ordered phase of the system and decreases to zero well into the disordered phase. It can be shown that, for sufficiently large system sizes, the Binder cumulants are rather insensitive to the system size, and their curves cross each other at the same point T_c , regardless of L , thus providing an estimate of the critical point in the thermodynamic limit ($L \rightarrow \infty$). Therefore, as determined by the common intercept of the curves for different system sizes we have found $T_c = 3.44 \pm 0.02$. This estimate is consistent with those obtained from the magnetization data, as well as with those signaled by the maxima in the susceptibility; see Fig. 3(b) and (c). For each L , the inflection point in m_L^b versus T provides the existence of second-order phase transitions occurring between ordered and disordered phase, and can be seen in Fig. 3(b).

In Fig. 4, we display the temperature dependence of the layers susceptibility χ_L^l , for several interlayer separations. Now, in the compact limit for $d = 1.0$, the peak in χ_L^l is located at $T_c \approx 3.44$ and as d increases, the critical temperature decreases. Notably, once the distance d between the layers surpasses 2.5, the layers act independently, halting the decrease in critical temperature.

We also studied the curves of m_L^l , U_L^l , and χ_L^l versus temperature T , as shown in Fig. 5, in the vicinity of the phase transition point. These quantities were obtained from the average value of each layer since the isolated layers presented the same critical behavior.

For a finite lattice, the system can transition between positive and negative magnetization states, and for a statistically large sample, the resulting magnetization is

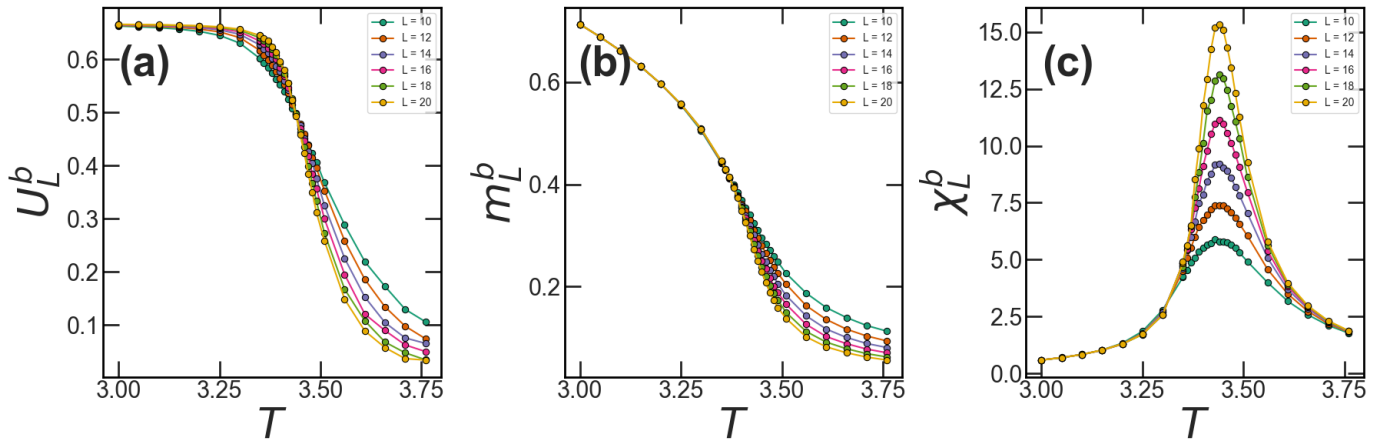


Figure 3. (a) Fourth-order Binder cumulant U_L^b , (b) magnetization m_L^b , and (c) susceptibility χ_L^b versus temperature T for several lattice sizes L , as indicated in the figures. The results were obtained for $\alpha = 1.0$, $d = 1.0$, $L_z = 10$, $N_b = 10L^2$. The critical temperature obtained by intersection of U_L^b (a) is given by $T_c = 3.44 \pm 0.02$. The error bars are smaller than the symbol size.

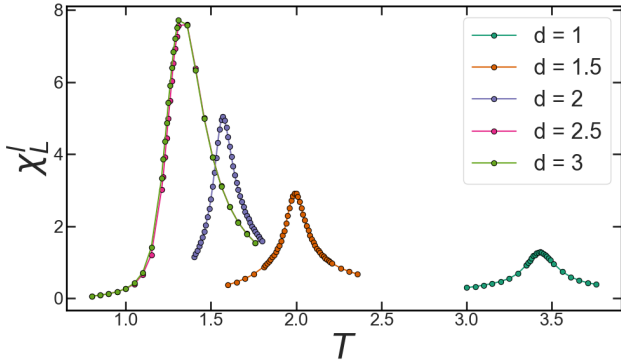


Figure 4. Bulk magnetic susceptibility χ_L^l versus temperature T for different values of interlayer separations d , as indicated in the figure. The results were obtained for $\alpha = 1.0$ and $L = 14$.

zero. As a result, magnetization is calculated using the average of the absolute value of the magnetic moment. When we consider a multilayer system, if the layers are close ($d < 2.5$), the interaction is strong enough to correlate all layers, as illustrated in Fig. 6(a). On the other hand, for $d > 2.5$, each layer can transition independently between positive and negative states, as shown in Fig. 6(b). In this case, it is not reasonable to calculate bulk magnetizations.

In Fig. 7(a), we present the critical temperature T_c^b as a function of the distance between layers of thickness d for a bulk system with the magnetic interaction given by Eq. (2). When, we compare these results with Fig. 4, can observe a rapid decay of T_c for increasing values of d . It is worth noting, and as showed in Fig. 6, that Fig. 7(a) only presents data up to $d = 2.0$, since from $d = 2.5$ onwards the layers are already disconnected and we no longer have the presence of critical bulk behavior. Fig.

7(b) illustrates the critical temperature T_c^l of the layers, demonstrating that T_c^l is similar to T_c^b for short values of d , and T_c^l equals tends to a constant value of the 2D model, with the specific α , for high values of d .

From the MC simulations, we can also evaluate the critical exponents. The finite-size scaling theory enables the extrapolation of data obtained from simulations of finite systems to the thermodynamic limit. Since one assumes that the thermodynamic quantities scale with the system size L , close to T_c , as a power of L multiplied by a nonsingular function of the ratio between the critical exponents. Therefore, we can calculate the critical exponents by analyzing the slope of the best fit in the log-log plot using the scaling relations described in Eqs. (8), (9), and (10). By examining the slope of the log-log plot for the magnetization m_L^l at the critical point for different lattice sizes L , as indicated in Eq. (8), we determined the ratio $-\beta/\nu$, as depicted in Fig. 8(a) for L_z stacked. Similarly, also for L_z stacked, the slope of the log-log plot of Eq. (9) provides us the ratio γ/ν , see Figs. 8(b). Additionally, for the ν exponent associated with the correlation length of the system, we employed the derivative of the Binder cumulant of the scaling relations described in Eq. (10), where its slope in the log-log plot yields the relation $1/\nu$, as illustrated in Figs. 8(c) for L_z stacked. In the same way, but for $L_z = L$, we have the best linear fit resulting in $-\beta/\nu$, γ/ν and $1/\nu$, presented in Figs. 8(d), 8(e), and 8(f), respectively.

Given our focus on the slope of the log-log plot, we adjusted the linear coefficients of the lines to separate them, making it easier for the reader to visualize the fits. In Tabs. I and II, we list the values of the critical exponents for different values of α and d , with the number

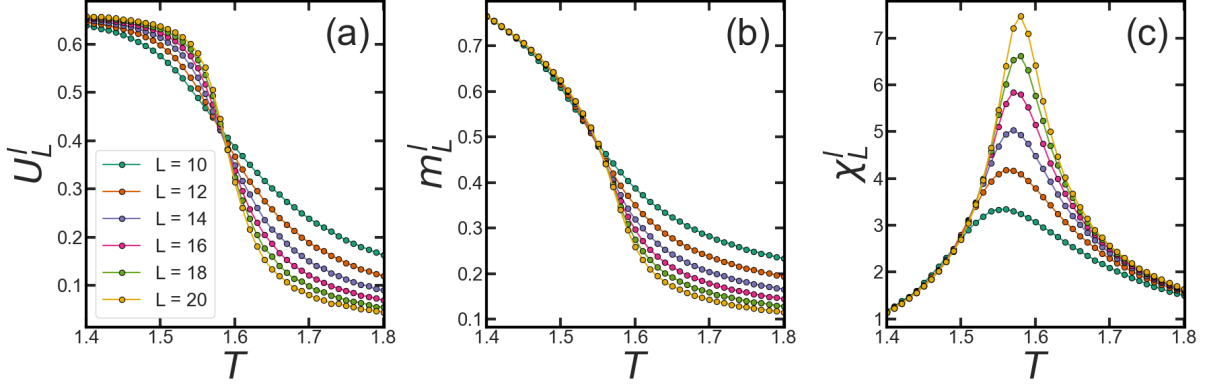


Figure 5. (a) Fourth-order Binder cumulant U_L^4 , (b) magnetization m_L , and (c) susceptibility χ_L^μ versus temperature T for several lattice sizes L , as indicated in panel (a). The results were obtained for $\alpha = 1.0$, $d = 2.0$, and with the exchange coupling given by Eq. (2). The critical temperature obtained of U_L^4 (a) is given by $T_c = 1.585 \pm 0.010$. The error bars are smaller than the symbol size.

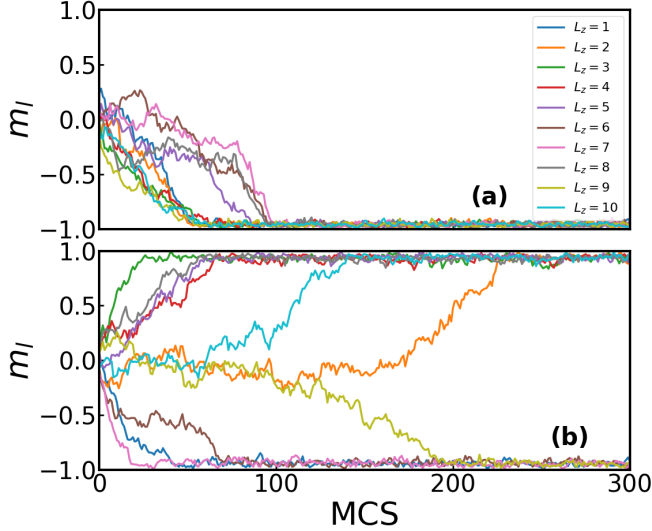


Figure 6. Layer magnetization m_L^l as a function of MCS for several lattice sizes L_z , as indicated in panel (a). The results were obtained for (a) $d = 2.0$ and (b) $d = 3.0$.

of layers $L_z = 10$ fixed ($N = 10L^2$). We also present in Tabs. III and IV the data for $L_z = L$, i.e., $N_b = L^3$ only for $\alpha = 1.0$, since not much difference was observed in the critical behavior of the system for different values of α when analyzing the system with fixed L_z .

Table I. Critical exponents β/ν , γ/ν , and $1/\nu$ for different values of α , d , with $L_z = 10$ ($N_b = 10N_l$).

α	d	T_c	β/ν	γ/ν	$1/\nu$
1.0	1.0	3.460 ± 0.010	0.490 ± 0.040	1.03 ± 0.02	1.09 ± 0.09
1.0	1.5	2.015 ± 0.005	0.450 ± 0.004	1.04 ± 0.02	1.43 ± 0.15
1.0	2.0	1.585 ± 0.010	0.390 ± 0.030	1.19 ± 0.05	1.73 ± 0.17
1.0	2.5	1.275 ± 0.010	0.140 ± 0.030	1.67 ± 0.10	1.11 ± 0.15
1.0	3.0	1.255 ± 0.005	0.134 ± 0.002	1.74 ± 0.02	1.01 ± 0.02
2.0	1.0	6.980 ± 0.010	0.480 ± 0.040	1.02 ± 0.02	1.08 ± 0.03
2.0	1.5	4.105 ± 0.005	0.500 ± 0.020	1.00 ± 0.02	1.35 ± 0.13
2.0	2.0	3.200 ± 0.010	0.420 ± 0.020	1.11 ± 0.03	1.63 ± 0.20
2.0	2.5	2.450 ± 0.020	0.190 ± 0.060	1.64 ± 0.15	1.39 ± 0.08
2.0	3.0	2.350 ± 0.005	0.137 ± 0.003	1.72 ± 0.03	0.99 ± 0.05
3.0	1.0	8.920 ± 0.020	0.460 ± 0.040	1.03 ± 0.02	1.08 ± 0.14
3.0	1.5	5.260 ± 0.010	0.480 ± 0.020	1.00 ± 0.01	1.32 ± 0.13
3.0	2.0	4.093 ± 0.003	0.410 ± 0.020	1.10 ± 0.03	1.60 ± 0.26
3.0	2.5	3.080 ± 0.010	0.210 ± 0.060	1.61 ± 0.13	1.47 ± 0.07
3.0	3.0	2.925 ± 0.005	0.142 ± 0.004	1.72 ± 0.03	0.99 ± 0.05

Table II. Critical exponents β/ν , γ/ν , and $1/\nu$ for different values of α , d , and $N_b = LN_l$.

α	d	T_c	β/ν	γ/ν	$1/\nu$
1.0	1.0	3.44 ± 0.02	0.30 ± 0.04	1.38 ± 0.06	1.06 ± 0.15
1.0	1.5	2.02 ± 0.01	0.36 ± 0.07	1.24 ± 0.02	1.08 ± 0.16
1.0	2.0	1.61 ± 0.01	0.41 ± 0.13	1.12 ± 0.12	1.31 ± 0.23
2.0	1.0	6.94 ± 0.01	0.29 ± 0.03	1.36 ± 0.05	1.00 ± 0.17
2.0	1.5	4.11 ± 0.02	0.37 ± 0.07	1.25 ± 0.02	1.07 ± 0.11
2.0	2.0	3.24 ± 0.02	0.45 ± 0.11	1.10 ± 0.08	1.11 ± 0.19
3.0	1.0	8.88 ± 0.03	0.30 ± 0.03	1.35 ± 0.04	1.08 ± 0.13
3.0	1.5	5.26 ± 0.02	0.36 ± 0.06	1.25 ± 0.02	1.02 ± 0.12
3.0	2.0	4.11 ± 0.02	0.28 ± 0.09	1.23 ± 0.02	1.10 ± 0.18

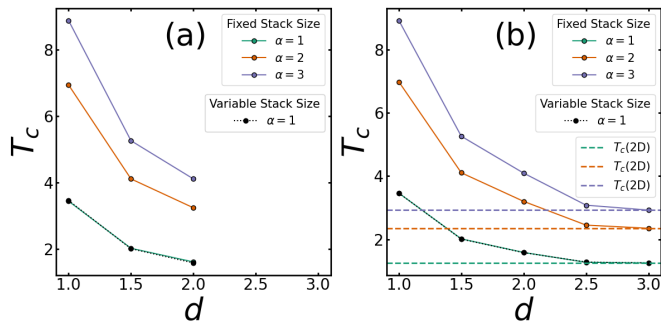


Figure 7. (a) Critical temperature multilayers T_c^b versus interlayer separations d for three different values of the parameter α , as indicated in the figure. (b) Critical temperature of the layers T_c^l versus interlayer separations d for three different values of the parameter α , as indicated in the figure. The dashed lines represent the critical temperature $T_c(2D)$ of the 2D system for $d \gg 3.0$.

Table III. Critical exponents β/ν , γ/ν , and $1/\nu$ for $\alpha = 1.0$ and different d , with $L_z = 10$ ($N_b = 10N_l$).

d	T_c	$-\beta/\nu$	γ/ν	$1/\nu$
1.0	3.460 ± 0.010	0.518 ± 0.007	0.957 ± 0.006	1.64 ± 0.11
1.5	2.008 ± 0.002	0.476 ± 0.020	1.05 ± 0.01	1.66 ± 0.08
2.0	1.580 ± 0.010	0.38 ± 0.04	1.22 ± 0.04	1.76 ± 0.05
2.5	1.280 ± 0.005	0.16 ± 0.03	1.72 ± 0.09	1.17 ± 0.05
3.0	1.255 ± 0.005	0.134 ± 0.001	1.74 ± 0.01	1.02 ± 0.01

We also conducted another analysis aimed at determining the universal functions of the magnetization Eq. (8) and the susceptibility Eq. (9). The data collapse technique establishes scaling and extracting associated critical exponents to equilibrium or non-equilibrium phase transitions in many systems. These scaling functions represent a data collapse [23] for a specific value of d and α , and various lattice sizes L . The critical exponents that best adjust the curves correspond to the possible critical exponents. For the values of T , we observe $\epsilon > 0$ (ferromagnetic phase) and $\epsilon < 0$ (paramagnetic phase), resulting in two branches in the data collapse, where the best collapse should occur near the critical point.

In this way, the data collapse was used here to verify whether the critical exponents, obtained from the linear fitting of the curves near the critical point as a function

Table IV. Critical exponents β/ν , γ/ν , and $1/\nu$ for $\alpha = 1.0$ and different d ($N_b = LN_l$).

d	T_c	$-\beta/\nu$	γ/ν	$1/\nu$
1.0	3.46 ± 0.01	0.514 ± 0.009	1.941 ± 0.01	1.62 ± 0.13
1.5	2.012 ± 0.002	0.45 ± 0.03	2.00 ± 0.01	1.57 ± 0.09
2.0	1.59 ± 0.01	0.51 ± 0.02	1.99 ± 0.02	1.65 ± 0.18

of the system's linear size in the log-log plot (see Fig. 8), are compatible with the system and describe the universality class of the system for the studied values of α and d . For this purpose, in Fig. 9 we present the collapsed curves using the exponents from Tables I and II, that is, for the system with fixed $L_z = 10$. Fig. 9 (a) shows the magnetization curves related to the average layer value, m_L^l , while Fig. 9 (b) shows the collapse of the susceptibility of this magnetization, χ_L^l . Similarly, but now for the thermodynamic quantities related to the bulk, in Fig. 9 (c) and (d) we present m_L^b and χ_L^b curves, respectively.

The verification of the exponents obtained from the linear fitting through data collapse was also performed for the case where $L_z = L$, i.e., the cubic system case. This is shown in Fig. 10, where panel (a) presents the curves of m_L^l , and panel (b) shows the curves of χ_L^l , both related to the layers. In Fig. 10 (c) and (d), for the bulk of the system, we present the curves of m_L^b and χ_L^b , respectively. In the analysis of the data collapse, we can see that the obtained exponents are consistent with the critical exponents, as both Fig. 9 and Fig. 10 provide good estimates of the scaling function near the critical point, since the curves for various system sizes merge into a single one in this regime.

We summarize the optimal values of the critical exponents, for the case with fixed $L_z = 10$, in a plot presented in Fig. 11. In Fig. 11(a) we display the critical exponents for different values of α and as a function of the interlayer distance d , considering the simulations based on the average values of individual layers. Fig. 11(b) corresponds to the bulk system. We can note from Fig. 11(a) that for almost all values of interlayer distance d (except $d = 2.5$), the different values of the parameter α share the same critical exponents, especially when d is greater than the imposed cutoff at 2.5. At this point, the layers become independent, and α , β , and γ converge to the 2D Ising exponents. When the layers are closer and the interactions more intense, significant changes occur in all critical exponents. In Fig. 11(b), we have the case of the bulk system with fixed $L_z = 10$, and even in the compact limit with $d = 1.0$, although β converges to the 3D Ising value, the average value of γ deviates slightly, and ν is far from the values identified in the literature.

With these results, we can observe that in the case where the layers are analyzed, for low values of d , the strong interaction between the layers changes the universality of the 2D system, such that we reach the critical dimension $D_c = 4$ of the Ising model. This is evident because at $d = 1$, $\beta \approx 0.5$, $\gamma \approx 1.0$, and $\nu \approx 1.0$ are the exponents of the mean-field approximation. However, as d increases, the interactions between the layers weaken and gradually modify the exponents until we reach the universality of the 2D Ising model, as the layers become isolated. When analyzing the bulk system, since we fixed

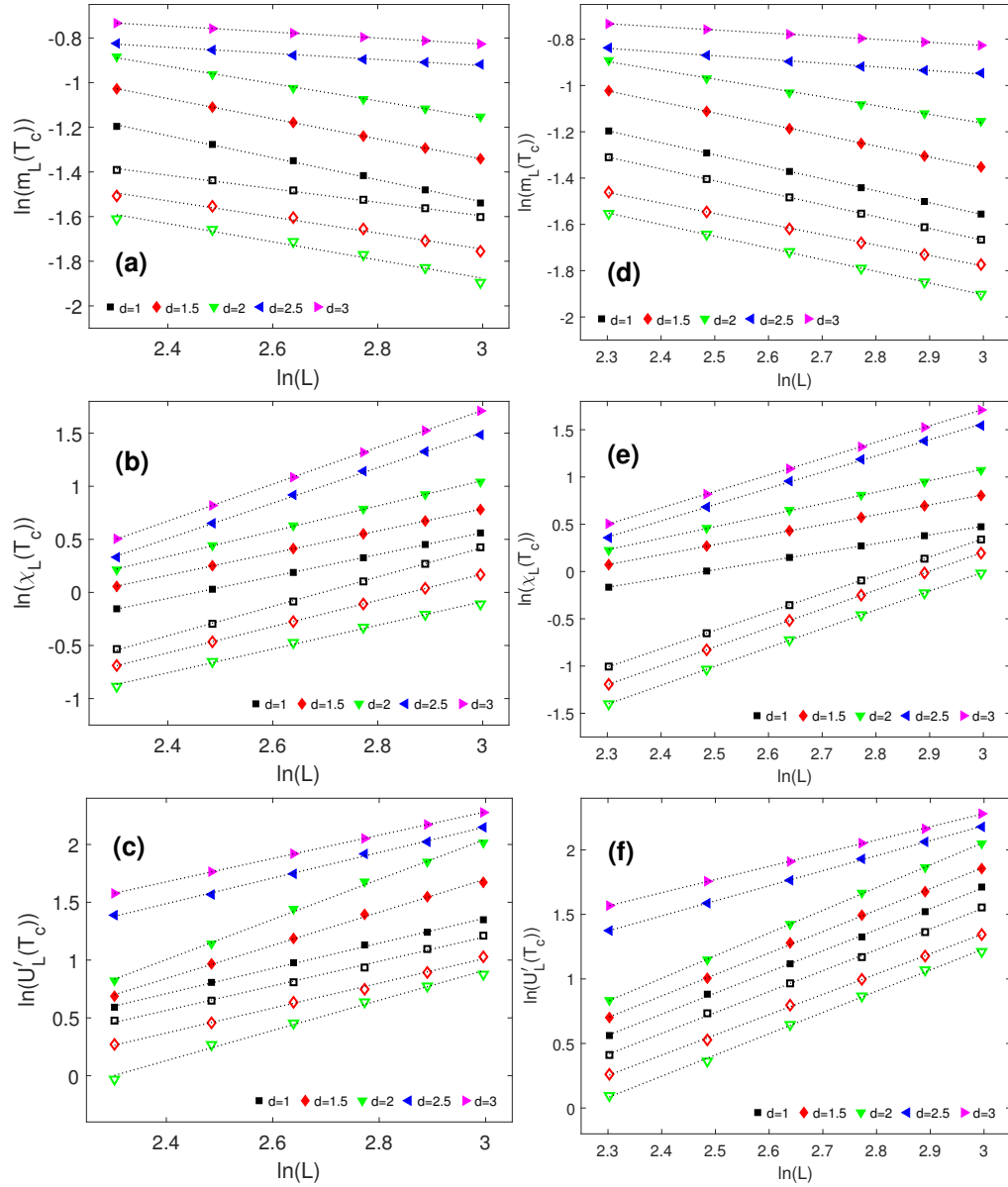


Figure 8. Log-log plots of $m_L^\mu(T_c)$, $\chi_L^\mu(T_c)$, and $U_L^\mu(T_c)$ versus L at the critical point and for different values of d , as presented in the figures. These results were obtained for $\alpha = 1.0$. Filled symbols represent the fits for the layers, $\mu = l$, and empty symbols refers to the bulk system, $\mu = b$. The dotted lines represent the best fit for the data points. From these slopes, we have obtained the critical exponents $-\beta/\nu$, γ/ν , and $1/\nu$ as can be seen in Tabs. I, II, III, and IV. The error bars are within the symbol size. The panels (a), (b), and (c) correspond to the system with $L_z = 10$ ($N_b = 10N_l$). The panels (d), (e), and (f) correspond to the system with $L_z = L$ ($N_b = LN_l$).

$L_z = 10$ but the layers keep changing in size, we do not have a well-defined linear size for the system, and the exponents are not fully compatible with the 3D Ising model.

Now, for the simulations performed with a variable $L_z = L$, the optimal values of the critical exponents are presented in Fig 12. This can be seen in Fig. 12(a) the critical exponents for $\alpha = 1.0$ as a function of the interlayer distance d , considering simulations based on the average values of individual layers, while Fig. 12(b) corresponds to the bulk system. From Fig. 12(a), it is easy to see that the critical exponents obtained as av-

erages from individual layers when L_z is variable show similar qualitative behavior to that when L_z is fixed (see Fig. 11(a)), even reaching the 2D critical exponents when layers become independent at $d = 3.0$, but not exhibiting mean-field critical behavior at $d = 1.0$, as the system now has a well-defined dimension, a cubic system. In Fig. 12(b), we can observe that when performing simulations with varying L_z and with periodic boundary conditions, the values of the 3D critical exponents are reached in the compact limit at $d = 1.0$ and the interaction between neighboring layers is intense enough to maintain these

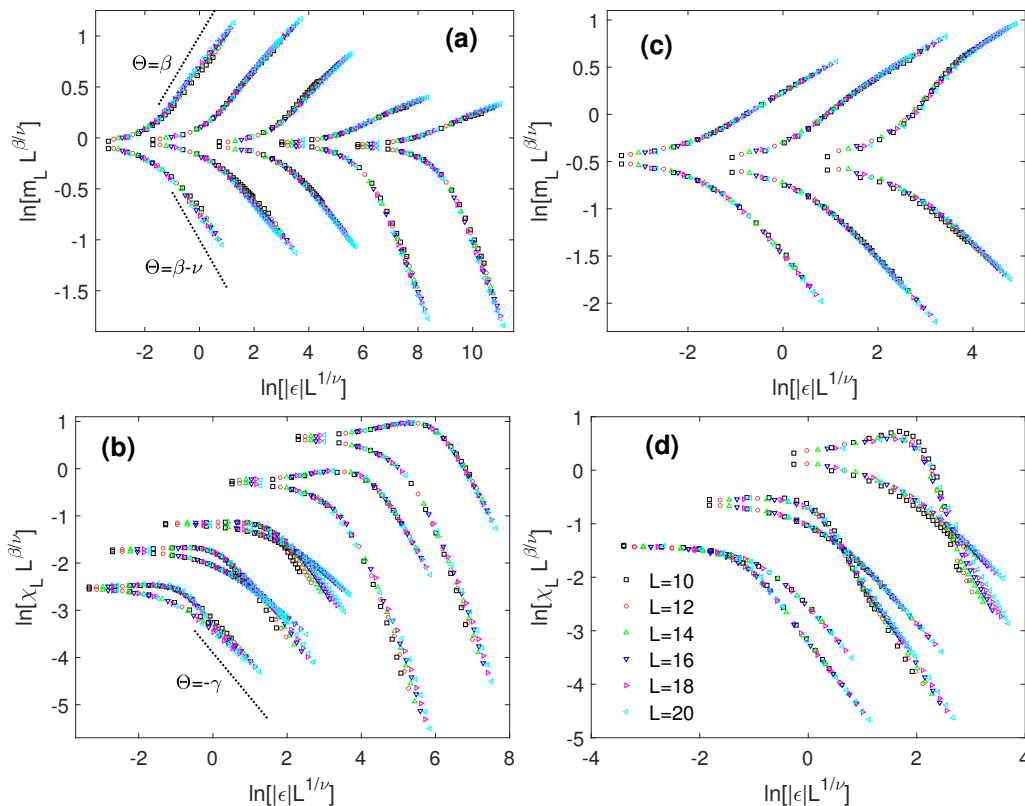


Figure 9. Data collapse near the critical point of the rescaled magnetization $m_L^b L^{-\beta/\nu}$ and susceptibility $\chi_L^b L^{\gamma/\nu}$ as a function of $|\epsilon| L^{1/\nu}$ for various d and L , as shown in panel (d). The panels (a) and (b) correspond to layers while those panels (c) and (d) correspond to the bulk. Additionally, in panels (a) and (c) the collapse sequence is from left to right for $d = 1.0, 1.5, 2.0, 2.5, 3.0$ and $d = 1.0, 1.5, 2.0$, respectively. In panels (b) and (d) the collapse sequence is from bottom to top for $d = 1.0, 1.5, 2.0, 2.5, 3.0$ and $d = 1.0, 1.5, 2.0$, respectively. The log-log plots were used to obtain the slope Θ of the asymptotic behavior of the scaling functions, where the straight-dashed lines represent this asymptotic behavior, as described by Eq. (9) and Eq. (9). Here, we used $\alpha = 1.0$ and $L_z = 10$ ($N_b = 10L^2$).

even at greater distances ($d = 2.0$).

IV. CONCLUSIONS

In this work, we have used MC simulations and the finite-size scaling theory to explore the critical behaviors and thermodynamic properties of a multilayer system. Our study specifically addressed how variations in the interlayer distance influence the magnetic coupling and the phase transitions in these systems. We conducted simulations with fixed and variable numbers of layers L_z , analyzing the behavior of the layers as well as the bulk system. For the fixed value of $L_z = 10$, the layers interact strongly in $1.0 \leq d \leq 2.0$, causing the exponents to deviate from the theoretical values for the 2D Ising model. However, in this case, since we do not have a well-defined dimension in the system, we find exponents similar to those of the mean-field approximation at $d = 1.0$. In this regime, it is also observed that the exponents do not have a strong dependence on α . As d increases and we reach the cutoff value ($d = r_{ij} = 2.5$), the exponents become more sensitive to the values of α . Nevertheless, when

$d > 2.5$, the layers become independent, and the critical exponents with different α values converge to those of the 2D Ising model. On the other hand, when analyzing the bulk system, the difference between the number of layers L_z and the layer sizes $N = L \times L$, prevents the system from exhibiting the universality class of the 3D Ising model, especially regarding the exponent related to the correlation length.

On the other hand, when varying L_z , so that we are now dealing with a cubic system, we have a well-defined dimension in the system. The critical exponent related to the correlation length, both in the case of the layers and in the bulk, converges to the value of the 3D Ising model in the range $1.0 \leq d \leq 2.0$. This change in the exponent ν prevents us from obtaining critical exponents resembling those of the mean-field approximation at $d = 1.0$ when analyzing only the layers. However, for $d > 2.5$, we still find exponents of the 2D Ising model, as in this regime the layers are isolated. Nevertheless, because both the number of layers and the layer sizes increase uniformly, in the bulk system analysis, we always find critical exponents of the 3D Ising model.

Finally, based on the data from Tables I and III, we

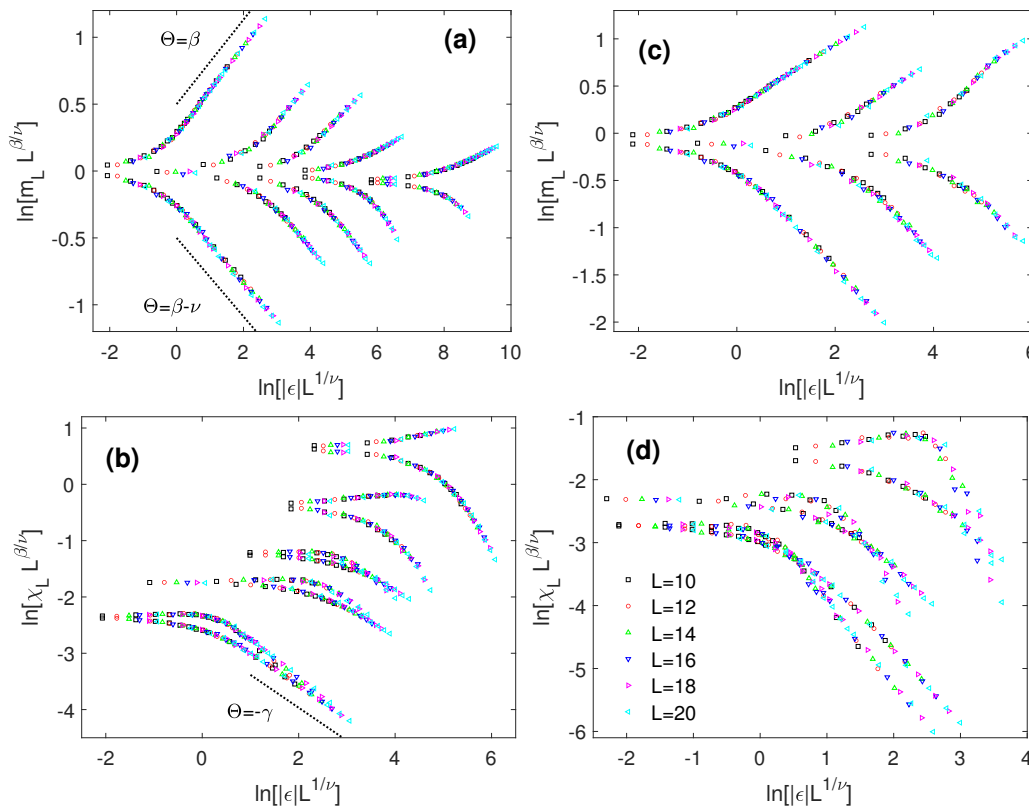


Figure 10. Data collapse near the critical point of the rescaled magnetization $m_L^\mu L^{-\beta/\nu}$ and susceptibility $\chi_L^\mu L^{\gamma/\nu}$ as a function of $|\epsilon| L^{1/\nu}$ for various d and L , as shown in panel (d). The panels (a) and (b) correspond to layers while those panels (c) and (d) correspond to the bulk. Additionally, in panels (a) and (c) the collapse sequence is from left to right for $d = 1.0, 1.5, 2.0, 2.5, 3.0$ and $d = 1.0, 1.5, 2.0$, respectively. In panels (b) and (d) the collapse sequence is from bottom to top for $d = 1.0, 1.5, 2.0, 2.5, 3.0$ and $d = 1.0, 1.5, 2.0$, respectively. The log-log plots were used to obtain the slope Θ of the asymptotic behavior of the scaling functions, where the straight-dashed lines represent this asymptotic behavior, as described by Eq. (9) and Eq. (9). Here, we used $\alpha = 1.0$ and $L_z = L$ ($N_b = L^3$).

can observe that the critical behavior of the layers system, whether with a fixed or varying L_z , shares a weak universality class, as the ratios of the exponents β/ν and γ/ν are equivalent, within the respective margins of error. However, the exponent ν depends on the behavior of L_z . On the other hand, the critical behavior of the bulk system, as seen in Tables II and IV, is significantly affected by whether L_z is fixed or varies with the layer sizes. We also observe a weak universality class relating both the layers and the bulk system, as in the regime $1.0 \leq d \leq 2.0$, there is a strong interaction between the layers, and both systems share the same value for the

exponent ν , within the appropriate margin of error.

ACKNOWLEDGMENTS

This work was financially supported by the Fundação Coordenação de Aperfeiçoamento de Pessoal de Nível Superior (CAPES), and Conselho Nacional de Desenvolvimento Científico e Tecnológico (CNPq) of Brazil (Process No. 140141/2024-3).

[1] M. N. Baibich, J. M. Broto, A. Fert, F. N. Van Dau, F. Petro, P. Etienne, G. Creuzet, A. Friederich, and J. Chazelas, Giant magnetoresistance of (001)fe/(001)cr magneticsuperlattices, *Phys. Rev. Lett.* 61, 2472 (1988).
 [2] G. Binasch, P. Grunberg, F. Saurenbach, and W. Zinn, Enhanced magnetoresistance in layered magnetic structures with antiferromagnetic interlayer exchange, *Phys.*

Rev. B 39, 4828 (1989).
 [3] P. Grunberg, S. Demokritov, A. Fuss, M. Vohl, and J. A. Wolf, *Journal of Applied Physics* 69, 4789 (1991).
 [4] S. Datta and B. Das, Electronic analog of the electrooptic modulator, *Applied Physics Letters* 56, 665 (1990).
 [5] Igor, J. Fabian, and S. Das Sarma, *Spintronics: Fundamentals and applications*, *Rev. Mod. Phys.* 76, 323

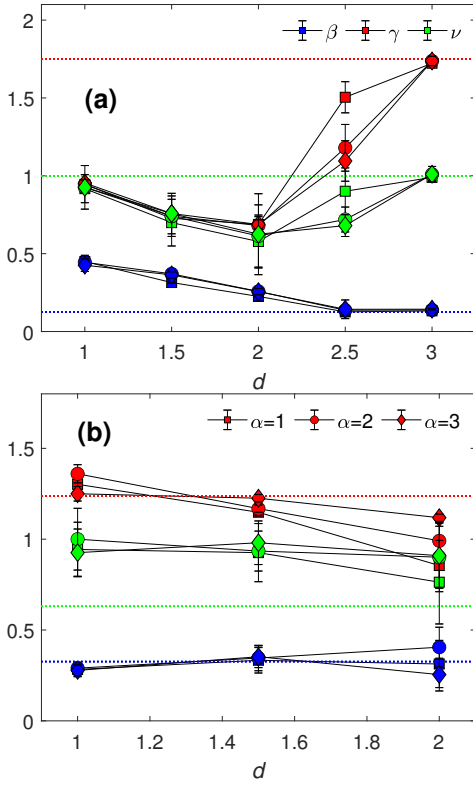


Figure 11. Critical exponents β , γ , and ν as a function of the interlayer distance d , and some values of α , as indicated in panel (b). The dashed red, green, and blue lines correspond, respectively, to the critical coefficients γ , ν , and β for the Ising model in 2D (a), and in 3D (b). Here, $L_z = 10$ and $N_b = 10L^2$.

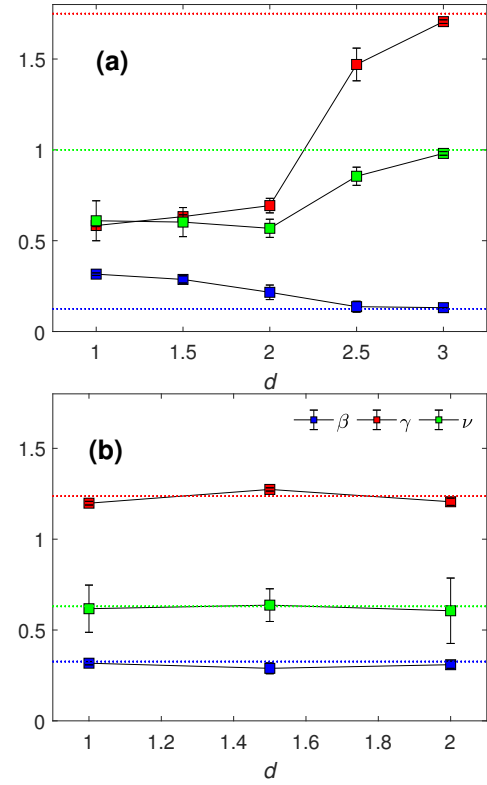


Figure 12. Critical exponents β , γ , and ν as a function of the interlayer distance d . The dashed red, green, and blue lines correspond, respectively, to the critical exponents γ , ν , and β for the Ising model in 2D (a), and in 3D (b). Here, $\alpha = 1.0$, $L_z = L$, and $N_b = L^3$.

- (2004).
- [6] T. Dietl, Lecture notes on semiconductor spintronics (2007), arXiv:0801.0145 [cond-mat.mtrl-sci].
- [7] T. Jungwirth, J. Sinova, J. Masek, J. Kucera, and A. H. MacDonald, Theory of ferromagnetic (iii,mn)v semiconductors, *Rev. Mod. Phys.* 78, 809 (2006).
- [8] F. Matsukura, H. Ohno, A. Shen, and Y. Sugawara, Transport properties and origin of ferromagnetism in (ga,mn)as, *Phys. Rev. B* 57, R2037 (1998).
- [9] H. Ohno, A. Shen, F. Matsukura, A. Oiwa, A. Endo, S. Katsumoto, and Y. Iye, (Ga,Mn)As: A new diluted magnetic semiconductor based on GaAs, *Applied Physics Letters* 69, 363 (1996).
- [10] M. Wang, R. A. Marshall, K. W. Edmonds, A. W. Rushforth, R. P. Campion, and B. L. Gallagher, Determining Curie temperatures in dilute ferromagnetic semiconductors: High Curie temperature (Ga,Mn)As, *Applied Physics Letters* 104, 132406 (2014).
- [11] R. K. Kawakami, E. Johnston-Halperin, L. F. Chen, M. Hanson, N. GuÃ©bels, J. S. Speck, A. C. Gossard, and D. D. Awschalom, *Appl. Phys. Lett.* 77, 2379 (2000).
- [12] M. Berciu and R. N. Bhatt, Effects of disorder on ferromagnetism in diluted magnetic semiconductors, *Phys. Rev. Lett.* 87, 107203 (2001).
- [13] M. P. Kennett, M. Berciu, and R. N. Bhatt, Monte carlo simulations of an impurity-band model for iii-v diluted magnetic semiconductors, *Phys. Rev. B* 66, 045207 (2002).
- [14] M. Berciu and R. N. Bhatt, Mean-field approach to ferromagnetism in (iii,mn)v diluted magnetic semiconductors at low carrier densities, *Phys. Rev. B* 69, 045202 (2004).
- [15] A. Richardella, P. Roushan, S. Mack, B. Zhou, D. A. Huse, D. D. Awschalom, and A. Yazdani, *Science* 327, 665 (2010).
- [16] K. Binder and D. W. Heermann, *Monte Carlo Simulation in Statistical Physics*, 3rd ed., Vol. 80 (Springer, Berlin, 1997).
- [17] D. Landau and K. Binder, *A Guide to Monte Carlo Simulations in Statistical Physics* (Cambridge University Press, Cambridge, 2000).
- [18] A. J. R. da Silva, A. Fazzio, R. R. dos Santos, and L. E. Oliveira, *J. phys.: Condens. matt., Journal of Physics: Condensed Matter* 16, 8243 (2004).
- [19] A. J. R. da Silva, A. Fazzio, R. R. dos Santos, and L. E. Oliveira, *Phys. Rev. B* 72, 125208 (2005).
- [20] M. Ruderman and C. Kittel, Indirect exchange coupling of nuclear magnetic moments by conduction electrons, *Physical Review* 96, 99 (1954).
- [21] T. Kasuya, A theory of metallic ferro- and antiferromagnetism on zener's model, *Progress of Theoretical Physics* 16, 45 (1956).
- [22] K. Yosida, Magnetic properties of cu-mn alloys, *Physical Review* 106, 893 (1957).
- [23] H. Stanley, Scaling, universality and renormalization: Three pillars of modern critical phenomena, *Rev. Mod.*

